Hydrodesulfurization of Thiophene in N-heptane Stream Using CoMo/SBA-15 and CoMo/AlSBA-15 Mesoporous Catalysts

Ana Carla S.L.S. Coutinho , Joana M.F. Barros , Marcio D.S. Araujo , Jilliano B. Silva , Marcelo J. B. Souza , Regina C.O.B. Delgado , Valter J. Fernandes Jr. , Antonio S. Araujo *

Posted Date: 29 January 2024

doi: 10.20944/preprints202401.1954.v1

Keywords: SBA-15; nanostructured materials; Cobalt; Molybdenum; hydrodesulfurization; environmental catalysis; petroleum refining

Article

Hydrodesulfurization of Thiophene in *n*-Heptane Stream Using CoMo/SBA-15 and CoMo/AlSBA-15 Mesoporous Catalysts

Ana Carla S. L. S. Coutinho [1], Joana M. F. Barros [2], Marcio D. S. Araujo [3], Jilliano B. Silva [4], Marcelo J. B. Souza [5], Regina C. O. B. Delgado [6], Valter J. Fernandes Jr. [7] and Antonio S. Araujo [8,*]

[1] Fluminense Federal University, School of Engineering, 24210-253, Niteroi RJ, Brazil; acoutinho@id.uff.br
[2] Federal University of Campina Grande, Center of Education and Health, Academic Unit of Biology and Chemistry, 58175-000, Cuite PB, Brazil; joana.barros@ufcg.br
[3] Federal University of Rio Grande do Norte, Institute of Chemistry, Post-graduate Program in Chemistry, 59078-970, Natal RN, Brazil; marcio.ifrn@gmail.com
[4] Federal University of Rio Grande do Norte, Post-graduate Program in Petroleum and Energy, 59078-970, Natal RN, 59078-970, Brazil; jilliano.lcl@gmail.com
[5] Federal University of Sergipe, Department of Chemical Engineering, 59078-970, Sao Cristovao SE, Brazil; marcelojbs@ufs.br
[6] Federal Rural University of Semi-Arid, 59625-900, Mossoro RN, Brazil; regina.brasil@ufersa.edu.br
[7] Federal University of Rio Grande do Norte, Institute of Chemistry, Laboratory of Fuels and Lubricants, 59078-970, Natal RN, 59078-970, Brazil; valter.fernandes@ufrn.br
[8] Federal University of Rio Grande do Norte, Institute of Chemistry, Laboratory of Catalysis and Petrochemistry, 59078-970, Natal RN, Brazil; antonio.araujo@ufrn.br
* Correspondence: antonio.araujo@ufrn.br

Abstract: The removal of sulfur from fossil fuels is one of the most important processes in modern refineries. It is accomplished via hydrodesulfurization (HDS) of the sulfur organic compounds in presence of heterogeneous catalysts. In the current work, heterogeneous catalysts containing cobalt and molybdenum supported on mesoporous materials type SBA-15 and AlSBA-15 were synthesized for application in the HDS reactions of thiophene in n-heptane stream. The mesoporous materials were synthesized by hydrothermal method starting from TEOS, pseudobohemite, hydrochloric acid and water. Pluronic P123 was used as template. The best calcination conditions for removal of the organic template were optimized by thermogravimetry analysis (TG/DTG). The calcined SBA-15 and AlSBA-15 supports were submitted to co-impregnation with solutions of cobalt nitrate and ammonium heptamolybdate, aiming the production of 15% in mass of metal loading with atomic ratio of [Co/(Co+Mo)]=0.45. The obtained materials were dried and calcined for obtaining the mesoporous catalysts in the form of CoMo/SBA-15 and CoMo/AlSBA-15. The catalysts were characterized by XRD, TG/DTG, SEM and nitrogen adsorption. From XRD analysis, it was verified that after decomposition of the cobalt and molybdenun salts, were formed MoO_3, Co_3O_4 and $CoMoO_4$ oxides on the supports, being attributed to these chemical species the activity for the HDS reactions. The activity of the obtained catalysts was evaluated in a continuously flowing tubular fixed-bed microreactor coupled on-line to a gas chromatograph, using n-heptane stream containing 12070 ppm of thiophene (ca. 5100 ppm of sulfur) as a model compound. From the catalytic tests it was verified that the synthesized catalysts presented good activity for the reaction, and the main obtained products were cis- and trans-2-butene, 1-butene, n-butane and low amounts of isobutane. The presence of 1,3-butadiene and tetrahydrothiophene (THT) were not detected. A mechanism of the primary and secondary reactions and subsequent formation of the olefins and paraffins, in the CoMo/SBA-15 and CoMo/AlSBA-15 mesoporous catalysts were proposed, considering steps of desulfurization, hydrogenation, dehydrogenation, THT decyclization and isomerization.

Keywords: SBA-15; nanostructured materials; cobalt; molybdenum; hydrodesulfurization; environmental catalysis; petroleum refining

 doi:10.20944/preprints202401.1954.v1

1. Introduction

1.1. Hydrotreating process

Currently, to comply with environmental legislation in many countries, there is great interest in developing processes to remove atmospheric contaminants, mainly sulfur derivatives, in addition to other hydrotreatment reactions. Classical catalysts used for such reactions in refining crude oil or liquid fuels generally consist of molybdenum supported on high surface area aluminas containing cobalt or nickel as promoters.

Hydrotreating processes (HDT) was developed from hydrogenation and cracking processes, and the most important HDT reaction was the removal of sulfur from the various fractions of petroleum and liquid coal derivatives, a process called hydrodesulfurization (HDS). Catalytic hydrotreatment consists of a variety of hydrogenation processes where oil and its various fractions react catalytically with hydrogen to remove S, N, O and metals. Nowadays, hydrotreating is widely used to convert heavy oil loads and to improve the quality of various products. It is used in the pretreatment of charges for other refining processes such as catalytic reforming, catalytic cracking (FCC) and hydrocracking catalyst (HCC). Such pre-treatment aims, among others, to protect the catalysts used in many consecutive stages in refining processes; reduce NO_x and SO_x emissions that may appear in the combustion of organic molecules, thus preventing premature corrosion of equipment; promote the improvement of the final properties of products from refineries (color, smell, stability, etc.) and add value to heavy distillates [1–3].

The use of increasingly heavier loads requires, in addition to hydrodesulphurization, conversion of larger molecules into smaller ones (hydrocracking - HCC), removal of metals (hydrodemetallization - HDM), nitrogen (hydrodenitrogenation - HDN), and in some cases, oxygen (hydrodeoxygenation - HDO). With the development of the petrochemical industry, other processes also gained prominence such as: aromatics degradation: hydrodearomatization (HDA); interconversion of organic molecules: isomerization (ISM); breaking of C-C bonds: hydrocracking (HCC) and olefin saturation: hydrogenation (HYD). Purification processes using hydrogen are applied to practically all distillate fractions. The complexity of the load and the lack of detailed knowledge about the nature of the compounds present in crude oil are one of the difficulties of hydrotreatment. It can be said that petroleum contains mainly hydrocarbons and, depending on its origin, may also contain large concentrations of heteroatoms [4–6].

The composition of the hydrotreatment charge varies widely depending on the origin of the oil. Sulfur is the most abundant of the heteroatoms present in crude oil, in general, ranging from 0.1 to 5% w/w. The content of nitrogen compounds present in petroleum varies from 0.1 to 1% w/w, and is generally concentrated in the heaviest fractions, mainly containing pyridine nuclei. Oxygen compounds are generally present in smaller quantities, values below 0.1% w/w, and are found in the forms of carboxylic acids and phenols. In Figure 1, some of the different types of aromatic compounds and sulfur-containing compounds commonly found in crude oil fractions are presented. The need to use increasingly heavier loads has led several countries in America and the European Union to increase efforts to control and prevent the emission of these pollutants. Thus, policies regulating the amounts of toxic compounds in fuels from refineries are being established. In Brazil, the National Agency of Petroleum, Natural Gas and Biofuels controls the concentration of sulfur in oil, gas and fuels.

The most industrially used HDS catalysts are based on Co(Ni)Mo/Al_2O_3, which have high mechanical strength and a large specific surface area [7–9]. The strong interactions between metals and alumina promote the formation of Mo-O-Al phases, resulting in an active phase for the process [10,11]. However, the phase formation between Co/Ni and Al_2O_3 is unfavorable for regulating the catalytic performance of MoS_2 sites. Active metal loading and unfavorable interactions have limited supported HDS catalysts to produce ultra-low sulfur fuels. Thus, several researches have been carried out aiming to improve the performance of HDS in relation to the following aspects: modification of zeolite supports, such as ZSM-5 [12–14] and Y zeolite [15], materials based on mesoporous silica, such as MCM-41, SBA-15 and SBA-16, [16–19], oxides single and mixed metallic [20–26] and carbon based

 doi:10.20944/preprints202401.1954.v1

materials [27–33]. However, the development of new catalysts containing well defined micro- and mesopores require further research and additional modifications for evaluation as new supports for ultra-deep desulfurization.

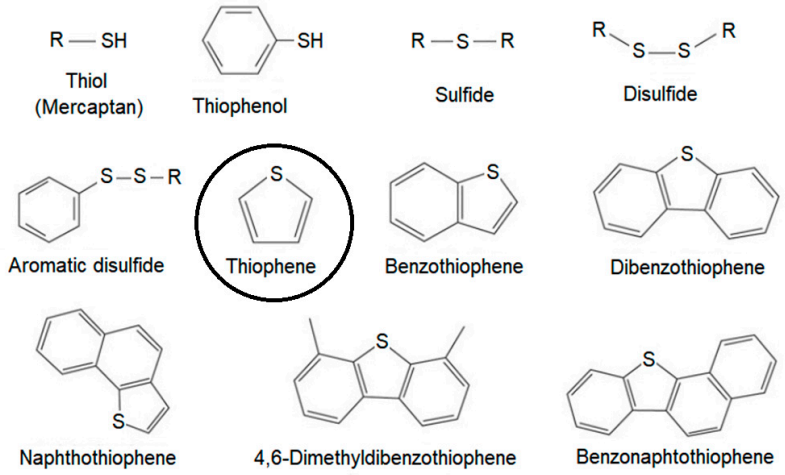

Figure 1. Some typical aromatic compounds and sulfur-containing compounds found in petroleum fractions, highlighting the molecular structure of thiophene.

Thiophene is a highly reactive molecule that contains a five membered ring consisting of four carbon atoms and one sulfur atom. Thiophene readily undergoes various reactions, including nucleophilic and electrophilic substitutions, cyclization, and oxidation. For this reason, it was chosen as probe molecule for this research.

This work aimed to propose the synthesis of hydrodesulfurization catalysts (HDS) based on mesoporous molecular sieves of the SBA-15 and AlSBA-15 containing cobalt and molybdenum oxides deposited on their surface. Typically, SBA-15 type mesoporous materials have a high specific surface area and large pore diameter, perfectly adaptable to the kinetic diameters of the largest sulfur compound molecules. These structural characteristics of the support are fundamental to maximize the metal dispersion of the active phases as well as improving the accessibility of the largest sulfur compounds, like thiophene, to metal sites, improving the efficiency to HDS processes.

2. Results and Discussion

2.1. Thermal Analysis of the Supports and Catalysts

Heat treatment or calcination is a very important step in obtaining high quality SBA-15 and AlSBA-15 mesoporous materials. In this step, all the P123 triblock copolymer used as a structure template is removed. Thermogravimetry is a technique used to determine the best calcination conditions, aiming to remove all organic material and preserve the well-ordered hexagonal structure. Figure 2 shows the TG and DTG curves for the SBA-15 and AlSBA-15 samples in non-calcined form at three different heating rates (β = 5, 10 and 20 ^{o}C/min).

As can be seen from the TG/DTG curves, three mass loss events were typically obtained, (Table 1). These events are attributed to: (i) range of 30-130 ^{o}C, desorption of physisorbed water in the pores of the material; (ii) range of 130-450 ^{o}C, removal of the directing molecules (P123) and (iii) range of 450-650 ^{o}C, residual removal of template and release of interstitial water resulting from the silanol condensation process. This behavior is typical for mesoporous materials, such as MCM-41 and SBA-15 [34–39].

 doi:10.20944/preprints202401.1954.v1

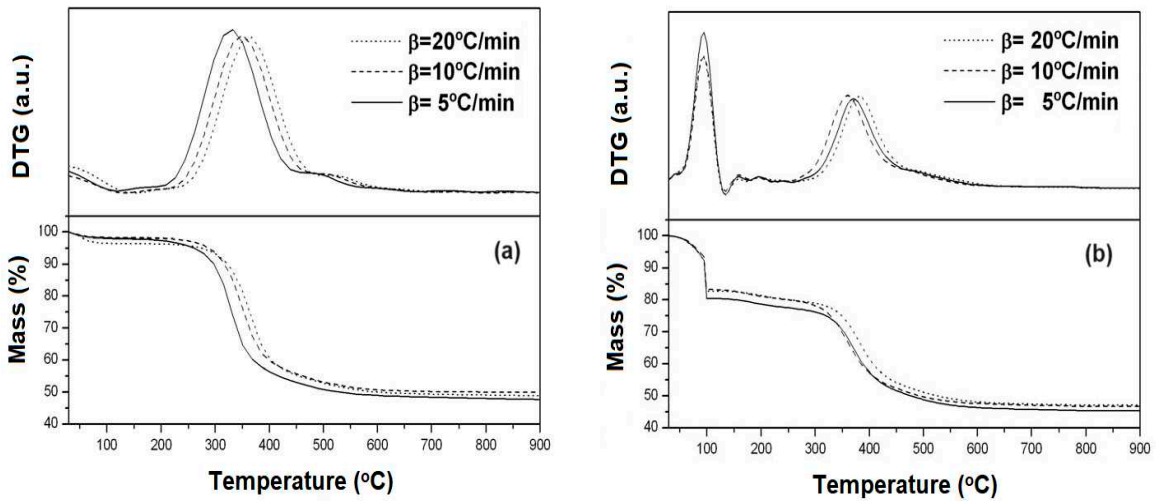

Figure 2. Thermogravimetry (TG) and Derivative Thermogrvimetry (DTG) curves for the mesoporous supports, at diferent heating rates: (a) SBA-15 and (b) AlSBA-15.

Table 1. Percentage of mass losses and respective temperature ranges for the samples SBA-15 and AlSBA-15 (Si/Al=50), at a heating rate of 10 °C/min.

Mesoporous	Temperature range (°C) and Mass loss (%)				
Material	30–130	130–450	450–650	30–650	30–900
SBA-15	2.1	45.2	3.9	51.1	52.2
AlSBA-15	12.9	32.8	5.6	51.3	52.7

According to the data in Table 1, it is observed that comparing the total mass loss from 30 to 900°C for the samples, there is no significant variation (from 52.3 to 52.7%), around 0.5% in mass. The difference in the percentage of mass loss among the materials relative to the first event, removal of physisorbed water in the pores of the materials, can be attributed to the humidity to which each sample was exposed before thermogravimetric analysis. Thus, the highest percentage of mass loss in the AlSBA-15 sample (Si/Al=50) may be related to physically adsorbed water, due the presence of aluminum, and the template removal, which would explain by the minor mass loss in the second event. The variation in the percentage of mass loss presented in the third event associated with the interstitial water may be an indication that the aluminum incorporated into the synthesis gel of the SBA-15 material interferes with the condensation of the silanol groups. Aluminum can be incorporated into the SBA-15 network both inside the network and on the surface of the material. The greater mass loss due to silanol condensation evidence that there is more aluminum on the surface of the materials.

It was also observed that increasing the heating rate, from 5 to 10 and 20 °C/min, the temperature shift to higher values, suggesting a variation of energy in the process for remotion of the P123 template from the pores of the materials. Thus, by applying multiple heating hate kinetic models [40–43], the values of the apparent activation energy (Ea) for this heat treatment process were in the range of Ea = 162–158 kJ/mol for SBA-15, and from Ea = 175–243 kJ/mol for AlSBA-15. The introduction of Al onto the SBA-1 5 structure suggests that Al^{3+} ions is present in the hexagonal structure, forming (-Si-O-Al-) interactions typical of aluminosilicate, consequently generating surface acid sites [44–49].

From the TG/DTG data, the temperature of 550 °C was selected for calcination of both materials. After the support calcination process, the active phases of cobalt and molybdenum were deposited on the mesoporous materials SBA-15 and AlSBA-15, using the excess solvent co-impregnation method. Thermogravimetry was also used to analyze the decomposition profiles of cobalt nitrate and ammonium heptamolybdate and thus determine the best conditions for calcining the catalysts. Figures 3 shows the TG/DTG curves of the decomposition of the precursor salts of Mo and Co supported on the SBA-15 and AlSBA-15 materials. The materials were calcined again in air

 doi:10.20944/preprints202401.1954.v1

atmosphere, to decompose the cobalt and molybdenum precursor salts into the respective oxides on the surface of the mesoporous supports and thus obtain the CoMo/SBA-15 and CoMo/AlSBA-15 supported catalysts.

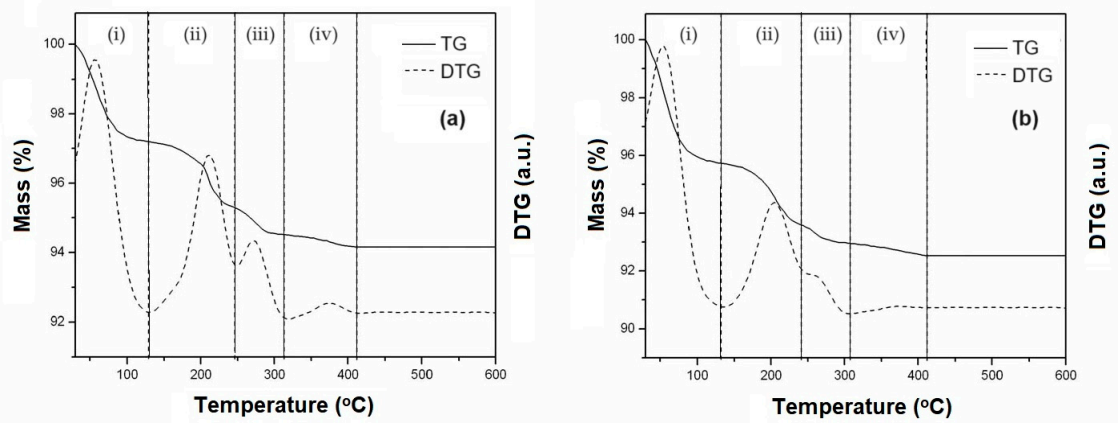

Figure 3. Thermogravimetry (TG) and Derivative Thermogravimetry (DTG) curves, obtained at heating rate of 10 °C/min showing the decomposition steps of Co and Mo salts for obtaining the supported mesoporous HDS catalysts: (a) CoMo/SBA-15 and (b) CoMo/AlSBA-15.

From TG/DTG curves (Figure 3), four mass loss events were observed in the following temperature ranges: (i) 30-130 °C, (ii) 130-240 °C, (iii) 240-310 °C and (iv) 310-410 °C, corresponding to steps for decomposition of the precursor salts inside the mesoporous supports SBA-15 and AlSBA-15. The values of mass loss relative to each step of decomposition are given in Table 2.

Table 2. Percentage of mass losses and respective temperature ranges for each step of decomposition of Co and Mo salts for obtaining CoMo/SBA-15 and CoMo/AlSBA-15.

Mesoporous Material	Temperature range (°C) and Mass loss (%)				
	(i) 30–130	(ii) 130–240	(iii) 240–310	(iv) 310–410	Total 30–410
CoMo/SBA-15	2.8	1.85	0.82	0.37	5.84
CoMo/AlSBA-15	3.14	2.76	0.95	0.51	7.36

From the obtained data, it was observed that up to 450°C the salts were completely decomposed on the surface of the materials, and this temperature was taken as a reference for thermal treatment. Thus, the calcination was carried out at this temperature under air atmosphere, flowing at 100 mL/min, in which the Co and Mo salts undergo complete decomposition generating the CoMo/SBA-15 and CoMo/AlSBA-15 HDS catalysts.

2.2. X ray diffraction

The X-ray diffractograms (XRD) of the materials obtained in calcined form were used to identify the hexagonal structure characteristic of mesoporous materials type SBA-15 [50,51]. Emphasis was placed on observing the obtaining of the three main diffraction peaks, referring to the crystalline planes, whose Miller index are (100), (110) and (200). Two more peaks are observed, whose Miller indices are (210) and (300) indicate excellent textural uniformity of the material [52]. The first three peaks are characteristic of a two-dimensional p6mm hexagonal symmetry, common to SBA-15 type materials [53,54]. Figure 4a,b show the X-ray diffractograms of mesoporous materials of SBA-15 and AlSBA-15 (Si/Al=50), respectively.

 doi:10.20944/preprints202401.1954.v1

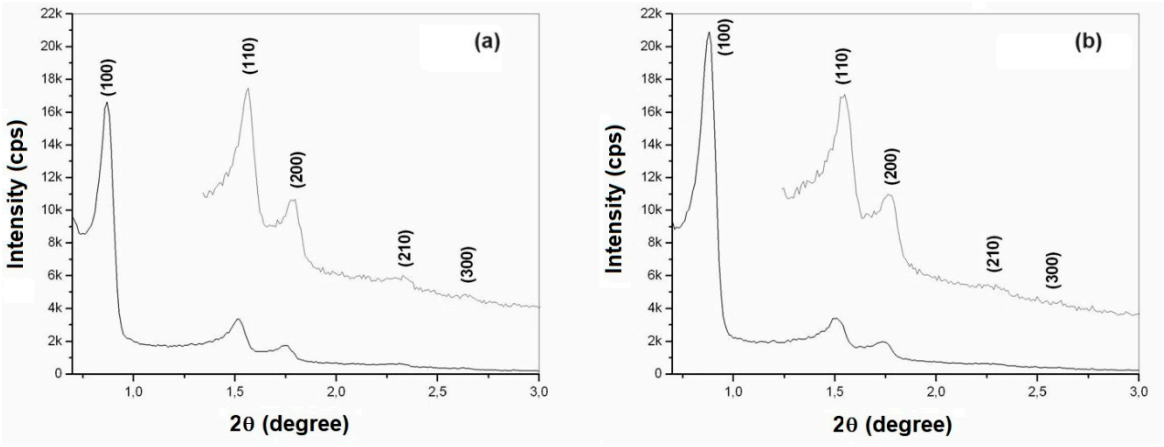

Figure 4. X-ray diffractograms of the calcined mesoporous materials: (a) SBA-15 and (b) AlSBA-15, showing the Miller indexes.

The XRD analysis of CoMo supported catalysts were carried out in two steps: low angle (0.5 to 5.0 degree) and high angle (5.0 to 60.0 degree), for observation of the ordered hexagonal phase and the presence of CoMo metal oxides, as shown in Figures 5 and 6, for CoMo/SBA-15 and CoMo/AlSBA-15, respectively.

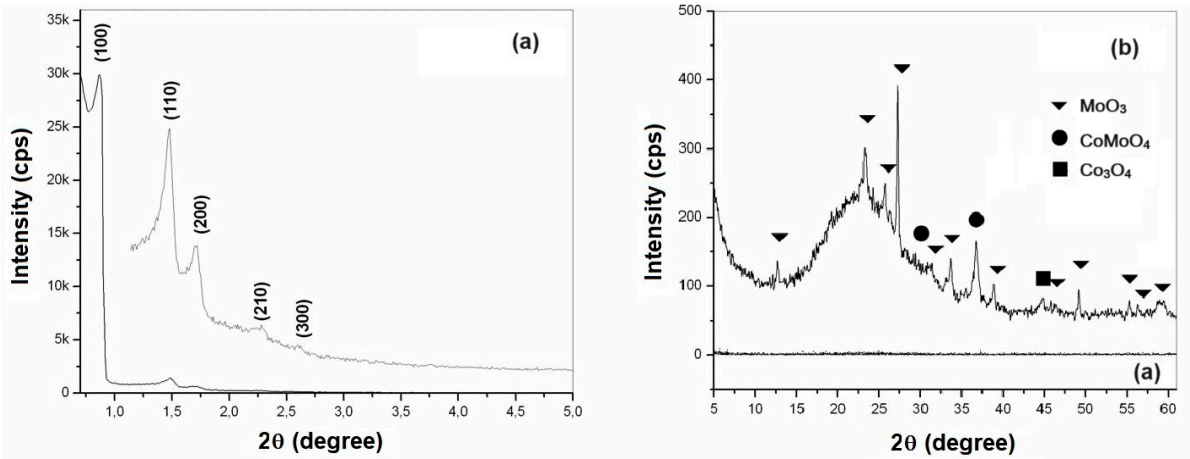

Figure 5. X-ray diffractograms of the calcined CoMo/SBA-15 obtained at low (a) and high (b) diffraction angles.

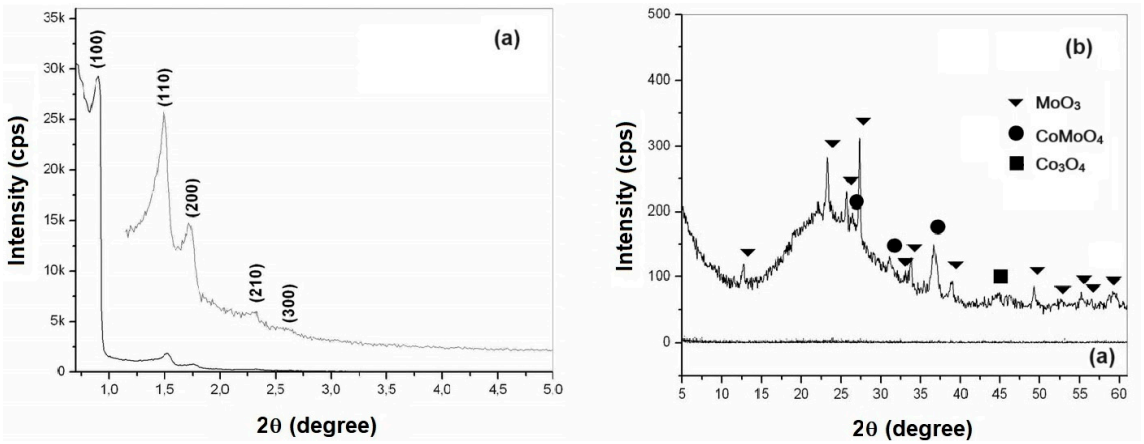

 doi:10.20944/preprints202401.1954.v1

Figure 6. X-ray diffractograms of the calcined CoMo/AlSBA-15 obtained at low (a) and high (a) diffraction angles.

From the diffractograms presented, the presence of the five main diffraction peaks was observed, whose Miller indices are (100), (110), (200), (210) and (300), indicating that high quality mesoporous materials with defined structure were obtained. well-ordered hexagonal [55]. The diffraction peaks for non-supported materials present better definition in relation to CoMo-supported, this fact is due to presence of heteroatom on the ordered structures. The mesoporous hexagonal arrangement parameter a_0 (lattice parameter) of the SBA-15 structure is obtained from the reflection peak for the (100) plane, which is the most characteristic in the X-ray diffractogram, which values are summarized in Table 3.

Analyzing the data on the mesoporous parameter (a_0) of the SBA-15 and AlSBA-15 supports from Table 3, it can be noted that in all cases there was a decrease in the value of this parameter. That value (a_o) represents the sum of the pore diameter (dp) and the silica wall thickness (wt). This decreasing may have probably occurred due to the deposition of nanoparticles of cobalt and molybdenum oxides inside the mesopores of the materials.

The crystalline phases of cobalt and molybdenum oxides were identified through the crystallographic charts of these oxides, found in the JCPDS (International Center of Powder Diffraction Standards) library. From research on crystallographic charts, were verified the presence of MoO_3 (JCPDS Registry: 35-06609) with an orthorhombic structure, Co_3O_4 (JCPDS Registry: 35-06609) with a cubic structure and mixed oxides of cobalt and molybdenum in the form of $CoMoO_4$ (JCPDS Registration: 21-0868) with monoclinic structure. The main peaks identified based on JCPDS were: MoO_3 (2Θ = 12.79; 23.32; 25.88; 27.32; 33.12; 33.72; 35.46; 38.96; 39.66; 38.96; 39.66; 45.76; 46.3; 49.26; 52.22; 54.13; 55.12; 56.36; 57.59 and 58.75), $CoMoO_4$ (2Θ = 26.40; 28.34; 31.98 and 36.63) and Co_3O_4 (2Θ = 18.93; 31.38; 36.92; 38.52; 44.97; 55.57 and 59.49). In all samples studied, the predominance of the crystalline phases MoO_3 and $CoMoO_4$ was observed. The presence of a diffraction peak at 44.97 degree, corresponding to Co_3O_4, was identified in all samples. Other cobalt and molybdenum oxides may also have occurred, but in very small quantities not identified from XRD due to interference with background radiation or because they are present in amorphous form.

Table 3. Crystallographic Properties of calcined SBA-15, AlSBA-15, CoMo/SBA-15 and CoMo/AlSBA-15 materials.

Materias	(hkl)	2 (degree)	$d_{(hkl)}$ (nm)	a_o (nm)
SBA-15	(100)	0.868	10.18	11.76
	(110)	1.516	5.83	
	(200)	1.748	5.05	
	(210)	2.313	3.82	
	(300)	2.630	3.36	
AlSBA-15	(100)	0.892	9.91	11.44
(Si/Al=50)	(110)	1.503	5.88	
	(200)	1.738	5.08	
	(210)	2.282	3.87	
	(300)	2.610	3.38	

 doi:10.20944/preprints202401.1954.v1

CoMo/SBA-15	(100)	0.873	10.12	11.69
	(110)	1.489	5.94	
	(200)	1.714	5.16	
	(210)	2.275	3.88	
	(300)	2.560	3.45	
CoMo/AlSBA-15	(100)	0.907	9.74	11.25
(Si/Al=50)	(110)	1.528	5.78	
	(200)	1.733	5.10	
	(210)	2.284	3.87	
	(300)	2.623	3.37	

2.3. Nitrogen Adsorption

The adsorption and desorption isotherms, as well as the distribution of pore diameters obtained for samples SBA-15 and AlSBA-15, are presented in Figures 7 and 8, respectively. It can be observed that type IV isotherms were obtained in the samples, according to the IUPAC classification, which are characteristics of mesoporous materials. According, and the hysteresis found are type I, characteristic of materials with a cylindrical pore system, or made from aggregates or clusters of spheroidal particles with pores of uniform size [56].

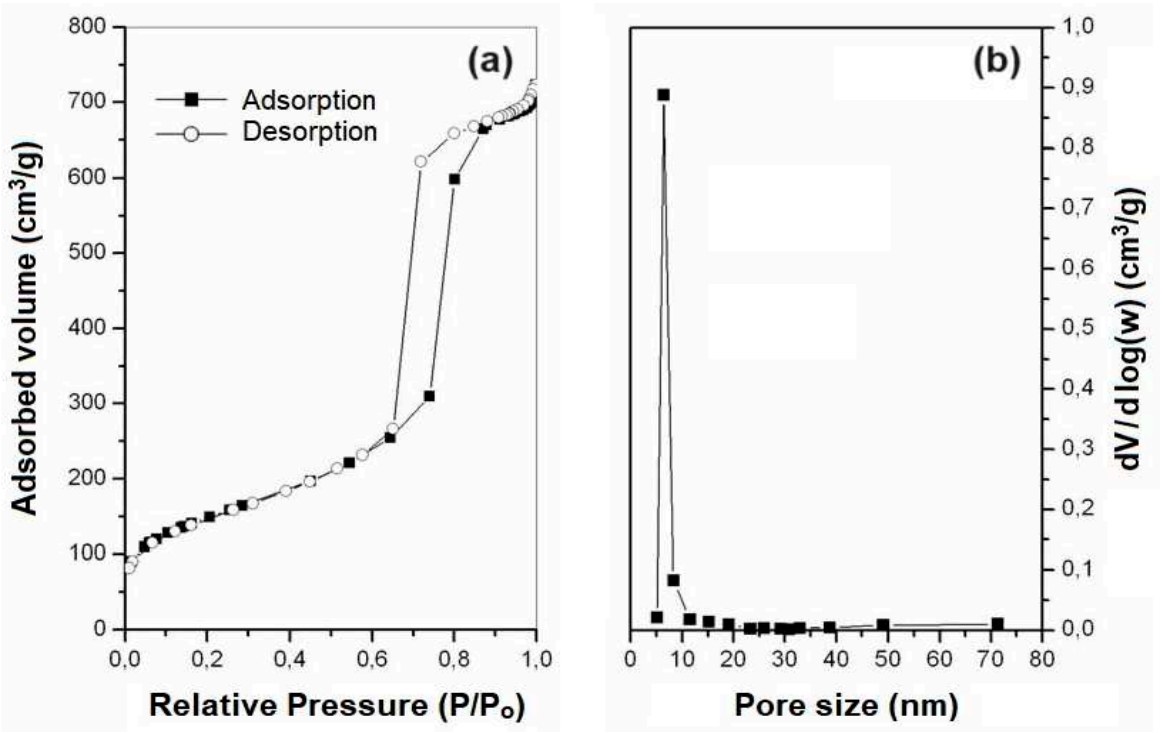

Figure 7. (a) N_2 adsorption isotherms and (b) pore size distribution of the SBA-15 mesoporous support.

 doi:10.20944/preprints202401.1954.v1

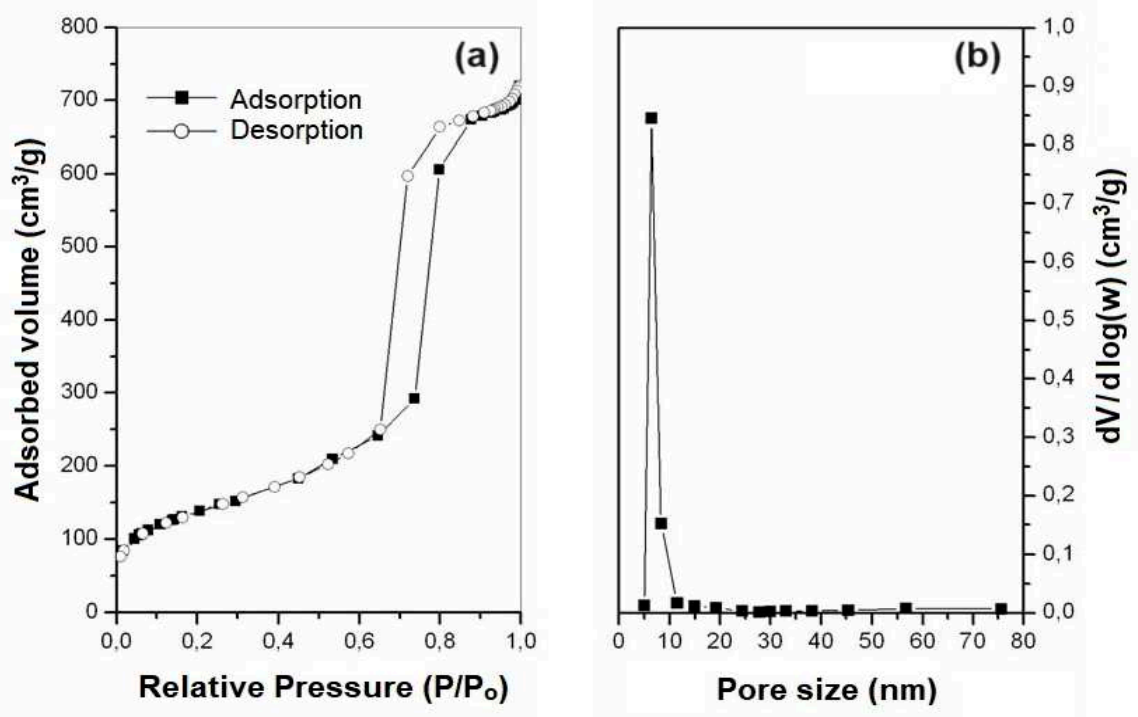

Figure 8. (a) N_2 adsorption isotherms and (b) pore size distribution of the AlSBA-15 mesoporous support.

The surface areas of the mesoporous materials obtained were determined from data on nitrogen adsorption isotherms at 77 K using the BET model [57] in the P/Po range of 0.05 – 0.20. The pore diameter distributions of mesoporous materials were obtained by the BJH method [58] correlating the desorbed volume values as a function of relative pressure (P/Po) in the algorithms, in a pore range of 1 – 80 nm. The average pore diameters were estimated through the pore distribution curves obtained by the BJH method and revealed values of 6.84 and 6.91 nm, for SBA-15 and AlSBA-15 (see Table 4), with low variation. After impregnation of Co and Mo metals, these values decreased for 6.11 and 6.82, respectively. As summarized in Table 4, the obtained materials presented pore volumes in the range of 0.84 a 1,12 cm^3/g. Using the BET method, it was observed that the samples had surface areas in the range of 402 to 602 m^2/g. These values are compatible with those found in the literature for SBA-15 containing aluminum [59,60].

Table 4. Surface properties of the mesoporous materials.

Sample	a_o (nm)	Dp (nm)	Wt (nm)*	Vp ($cm^3\ g^{-1}$)	S_{BET} ($m^2\ g^{-1}$)
SBA-15	11.76	6.84	4.92	1.12	602
AlSBA-15	11.44	6.91	4.53	1.07	495
CoMo/SBA-15	11.69	6.11	5.58	0.95	406
CoMo/AlSBA-15	11.25	6.82	4.43	0.84	402

a_o: mesoporous parameter; Dp: Pore diameter; Wt: Wall thickness *(Wt = a_o – Dp); Vp: Pore volume, obtained from BJH method.

It was observed that there was a decreasing in the mesoporous parameter, sum of the average pore diameter (Dp) and the silica wall thickness (Wt), with the introduction of Al on the support. The average pore diameter did not vary significantly with the introduction of Al. The average values of

 doi:10.20944/preprints202401.1954.v1

the silica wall thickness (Wt) can give these materials high mechanical resistance and possibility for application as catalytic supports in processes oil refining, where catalysts are often subjected to operating conditions with high temperatures and pressures [61,62].

After the impregnation of cobalt and molybdenum oxides on the supports, there were no changes in the shapes of the adsorption and desorption isotherms, continuing to be type IV, thus maintaining the mesoporous structure. The average pore diameter decreased with the introduction of Al into SBA-15. With the introduction of Co and Mo metals, the pore volumes were 0.95 and 0.84 cm3 g-1, and surface areas of 406 and 402 m2g-1, for CoMo/SBA-15 and CoMo/AlSBA-15, respectively, and a decreasing in the total surface area in relation to the mesopore supports was observed.

2.4. Scanning Electron Microscopy

Scanning electron micrographs, obtained at magnifications of 15000X, of the SBA-15 and AlSBA-15 materials are shown in Figure 9. The micrographs of CoMo/SBA-15 and CoMo/AlSBA-15 with details of the pore systems are shown in Figures 10 and 11, respectively. The SEM analyzes were carried out with the aim of observing the morphology of the synthesized nanostructured materials. It can be seen in the figures that silica fibers with micrometric dimensions are formed from the linear adhesion of nodules of submicrometric particles. The morphology of the AlSBA-15 (samples with Si/Al=50) was similar to the SBA-15 sample, even after impregnation of Co and Mo. In all cases, non-uniform fibers were observed, giving the appearance of "intertwined bead necklaces" [63–65], indicating that this is probably the phase corresponding to SBA-15, since XRD and nitrogen adsorption analyzes showed that these samples are pure and have a high degree of ordering, and good porosity, as viewed in Figures 10 and 11.

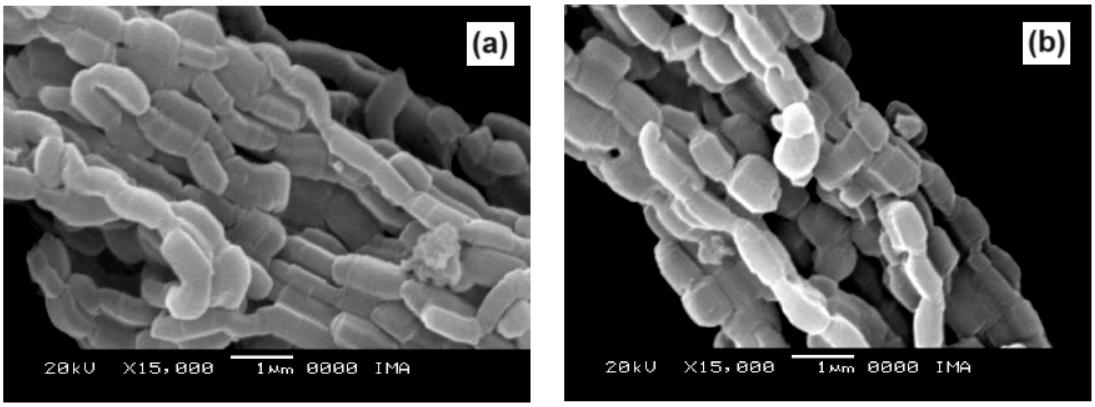

Figure 9. Scanning electron micrographs of the mesoporous supports: (a) SBA-15 and (b) AlSBA-15 (Si/Al=50).

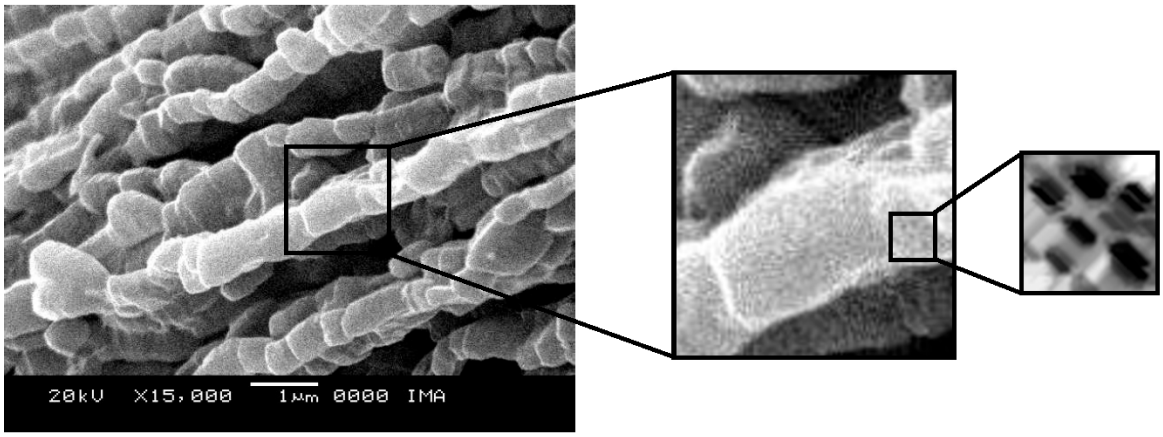

 doi:10.20944/preprints202401.1954.v1

Figure 10. Scanning electron micrograph of the mesoporous CoMo/SBA-15 catalyst showing details of porosity.

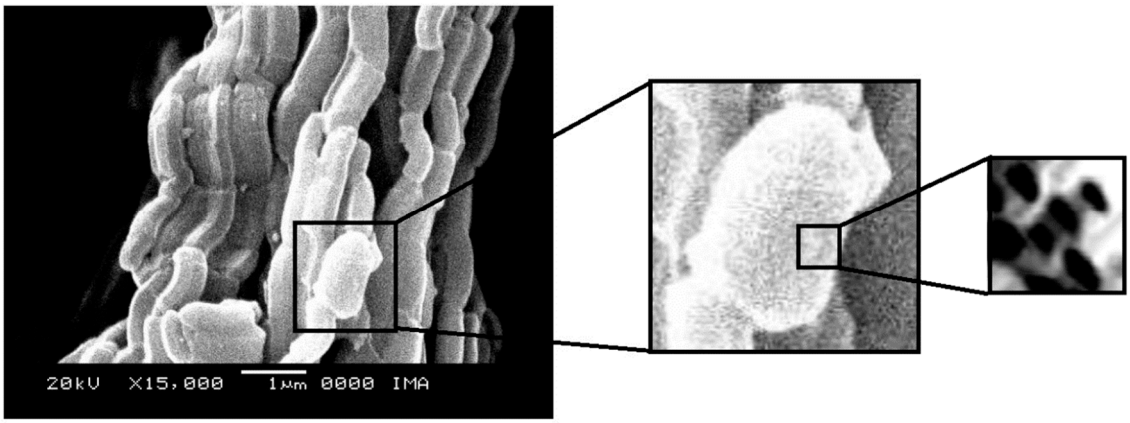

Figure 11. Scanning electron micrograph of the mesoporous CoMo/AlSBA-15 catalyst showing details of porosity.

In hydrodesulfurization reactions, MoO_3 and $CoMoO_4$ species can, during the HDS and sulfidation steps, transform into the MoS_2 and "CoMoS" phases, which are active and stable for the reaction. The presence of Co_3O_4 can give rise to Co_9S_8, a phase that is very inactive for HDS catalysts, but can also be reduced to metallic cobalt, which, properly accommodated at the ends of MoS_2 crystals, giving rise to active phases, known as "CoMoS" [66–68].

2.5. Catalytic Activities of CoMo/SBA-15 and CoMo/AlSBA-15

Before starting the catalytic tests for hydrodesulfurization of thiophene, some preliminary tests were carried out with the aim of verifying the occurrence of thermal cracking reactions under the operating conditions of the tests. The first test consisted of the mixture of 13500 ppm of thiophene (ca. 5100 ppm of Sulfur) in n-heptane steam through the reactor at 350°C without catalyst, with the aim of observing the occurrence of thermal degradation of the mixture at this temperature, which was not observed, where the chromatogram showed only the peaks relating to thiophene and n-heptane. The second test was conducted to verify the occurrence of catalytic cracking of pure n-heptane on the catalytic bed at 350°C containing the obtained catalysts. Once again, no peaks other than n-heptane were detected, proving that there was no catalytic cracking under these conditions. After preliminary tests, catalytic hydrodesulfurization tests (HDS) of the mixture of 13500 ppm of thiophene in n-heptane (ca. 5100 ppm of sulfur) were carried out with the objective of evaluating the conversion and selectivity of 15%CoMo/SBA-15 and 15%CoMo/AlSBA-15 catalysts (Si/Al=50). According to chromatograms, H_2S and C_4-hydrocarbon compounds were typically obtained in the following elution order: isobutane, 1-butene, n-butane, trans-2-butene and cis-2-butene. The presence of butadiene or isobutene was not observed. In thiophene HDS reactions, butadiene can occur as a primary reaction product or act as an intermediate to obtain butenes through a hydrogenation reaction, thus having a very short lifetime in the catalytic cycle and not appearing in appreciable quantities in product distribution [69]. In the case of isobutene, this product is thermodynamically unfavorable, with the conversion of linear butenes being preferred.

Figure 12a,b show the conversion and paraffin/olefin ratio, respectively, for HDS reactions on catalysts with 15% cobalt and molybdenum metal phase supported on SBA-15, AlSBA-15 (Si/Al=50). Figure 13a,b show the selectivity for the products.

It was observed that in the first 15 minutes of reaction the highest conversion values were obtained for all catalysts studied, these conversions progressively decreased until reaching stability normally after 60 minutes of reaction. Considering the conversion values obtained in 120 minutes of reaction, the CoMo/SBA-15 was more active than CoMo/AlSBA-15. Also, it was observed that after 60 min of reaction, the paraffin/olefin ratio increased for CoMo/SBA-15, whereas with the

 doi:10.20944/preprints202401.1954.v1

CoMo/AlSBA-15, this ration was almost constant, with values bellow 0.1. Through X-ray diffraction analyses, no diffractions of amorphous phases of MoO_3 nor other diffractions related to Co_3O_4 were observed other than that found for all samples. According to previous report [70], cobalt appears as a promoter for the hydrogenolysis reactions of the C-S bonds of thiophene, but it can also act as a promoter for other reactions such as isomerization and hydrogenation of butadiene after the HDS catalytic cycle. This promoting effect of cobalt can be attributed to the transfer of electrons to molybdenum oxide, reducing its oxidation state from Mo^{+6} to Mo^{+4}.

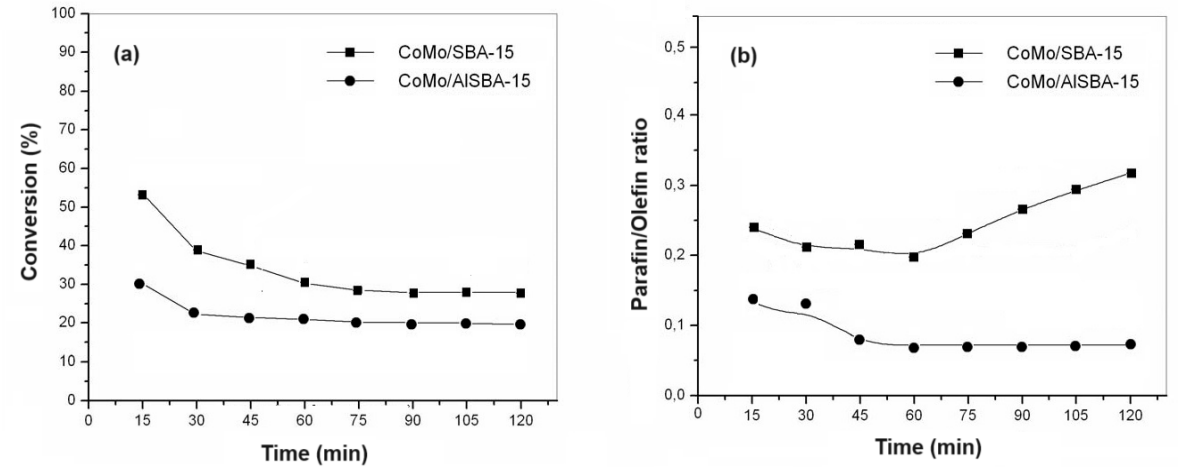

Figure 12. Catalytic activity for the CoMo/AlSBA-15 and CoMo/AlSBA-15 catalysts: (a) Conversion as a function of reaction time, and (b) paraffin/olefin ratio as a function of reaction time.

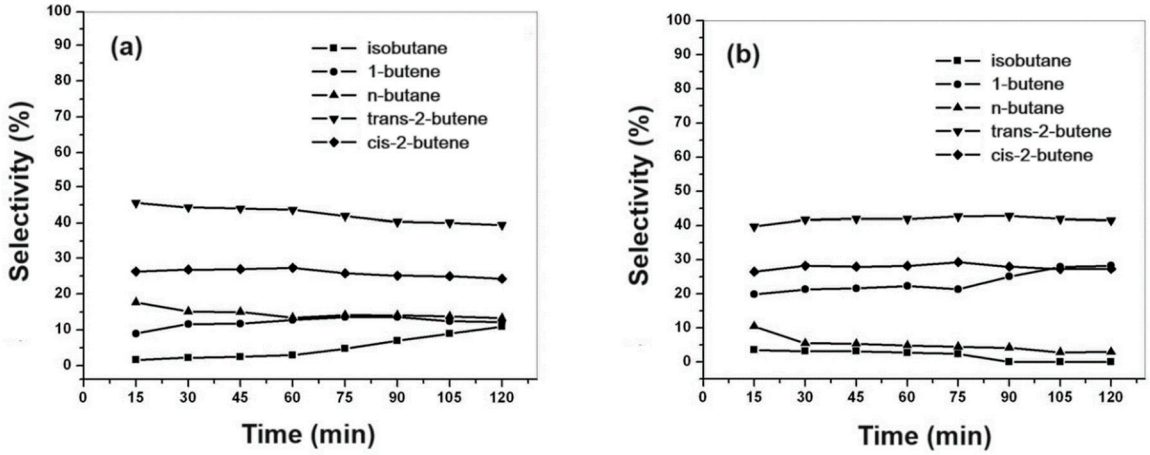

Figure 13. Product selectivity to paraffins and olefins as a function of reaction time for the mesoporous catalysts: (a) CoMo/SBA-15 and (b) CoMo/AlSBA-15.

A proposed reaction mechanism of thiophene on MoO_3 consider that the formation of butenes and n-butane can occur directly through one or two butadiene hydrogenation steps, forming 1-butene or n-butane, respectively [71]. Through the isomerization of 1-butene it is possible to obtain cis-2-butene and trans-2-butene by displacing the double bond. Isobutane can be obtained through chain isomerization of n-butane. The presence of 1,3-butadiene and tetrahydrothiophene (THT) molecules were not detected. Thus, it is supposed that these compounds suffer interconversion reactions inside the mesoporous of the CoMo/SBA-15 and CoMo/AlSBA-15 catalyst, as schematized in the Figure 14.

 doi:10.20944/preprints202401.1954.v1

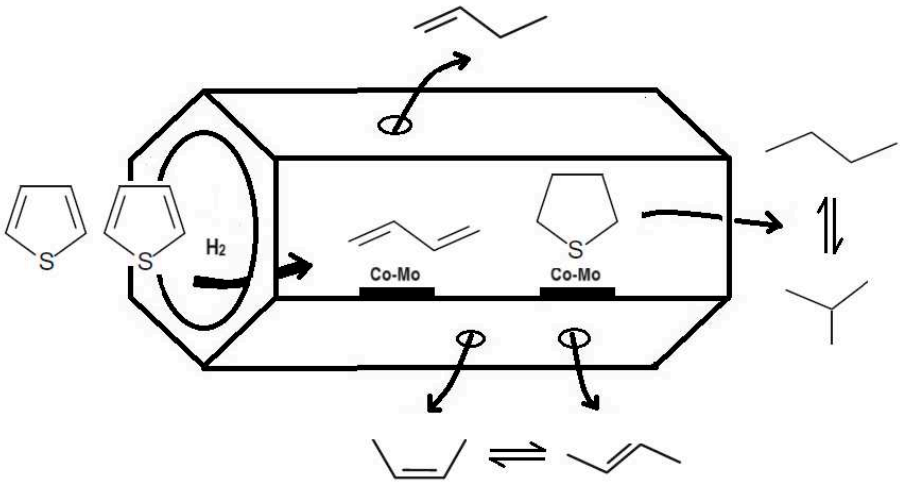

Figure 14. Possible HDS thiophene reaction inside the mesopore system of the CoMo/SBA-15 and CoMo/AlSBA-15 catalysts, and desorption of the products.

According to the obtained results, it was proposed that thiophene molecules suffer desulfurization in presence of hydrogen to form 1,3-butadiene, and hydrogenation to form tetrahydrothiophene (THT). In presence of Co and Mo metals, 1,3-butadiene reacts with hydrogen, to obtain 1-butene and 2-butene, and this suffers isomerization to cis- and trans-2-butene. The THT species are adsorbed on Co-Mo metals and a new step of desulfurization is suggested, to formation of paraffins n-butane, and a subsequent isomerization to isobutane. The selectivity for n-butane suggests that it forms via secondary reactions of primary products. Therefore, after one hour of reaction, using the CoMo/SBA-15 catalyst, the isobutane selectivity increased with n-butane decreasing with reaction time, suggesting a step of isomerization. For the CoMo/AlSBA-15 catalyst, this behavior was not observed, indicating that the presence of aluminum, generating Bronsted acid sites, stabilizes the structure, and inhibits the paraffin isomerization. From the conversion, selectivity and paraffin/olefin ration, a mechanistic scheme for thiophene HDS is proposed in Figure 15, showing a sequence of primary and secondary reactions.

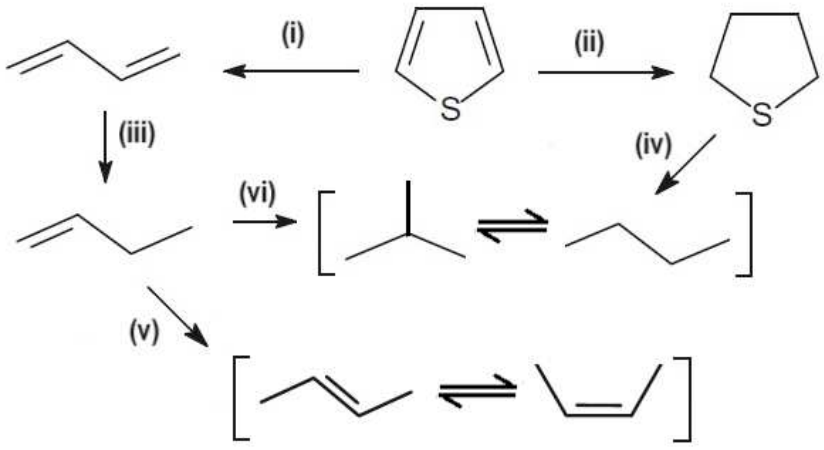

Figure 15. Proposed mechanism reaction for hidrodessulfurization of thiophene using the mesoporous CoMo/SBA-15 and CoMo/AlSBA-15 catalysts, showing steps: (i) desulfurization; (ii) hydrogenation; (iii) skeletal hydrogenation; (iv) desulfurization and decyclization; (v) cis- and trans-isomerization; (vi) hydrogenation and C_4-paraffins isomerization.

3. Materials and Methods

 doi:10.20944/preprints202401.1954.v1

3.1. Synthesis of the SBA-15 and AlSBA-15 supports.

The CoMo/SBA-15 and CoMo/AlSBA-15 catalysts were synthesized in two steps: (i) hydrothermal synthesis and calcination of the supports; (ii) impregnation of the Co and Mo on the obtained supports.

The hydrothermal synthesis of mesoporous supports of type SBA-15 and AlSBA-15 with molar ratio Si/Al=50, were synthesized using the following reagents: tetraethylorthosilicate (TEOS, Sigma-Aldrich, 98% - $Si(OC_2H_5)_4$); Pseudobohemite (AlOOH, Vista, 70% Al_2O_3 and 30% water); Pluronic P123 (Triblock Copolymer, BASF Co., average PM = 5750 g/mol); hydrochloric acid (Merck, HCl, 37% vol.) and distilled water. The hydrothermal syntheses were carried out using 250 mL Teflon autoclaves wrapped in a stainless steel protection manufactured by Parr Instruments.

The reagents were mixed to obtain a reactive hydrogel with molar composition: 0.017 P123 : 1.0 TEOS : 5.7 HCl : 193 H_2O [72]. First, the P123 template was dissolved in distilled water and HCl, with stirring and heating to 35°C. Once the temperature was reached, the silica source, tetraethylorthosilicate (TEOS), was added. The mixture was kept under stirring and heated at 35°C for 24 hours (pH = 0-1) to obtain a homogeneous gel. Then it was transferred to the autoclave and stored in an oven for 48 hours, previously heated to 100°C. For the AlSBA-15 support, the reagents were mixed to obtain a reactive hydrogel with the following molar composition: 0.017 P123 : 1.0 TEOS : xAl_2O_3 : 5.7 HCl : 193 H_2O. The value of "x" was used to maintain the molar ratio Si/Al=50.

Once the hydrothermal syntheses were completed, the materials obtained were vacuum filtered and washed with 50 mL of a 2% solution by volume of hydrochloric acid in ethanol. This procedure facilitates the removal of the organic director from the pores of the material, reducing calcination time. After this procedure, each material was placed to dry at room temperature for 24 hours. To completely remove P123 from the pores of mesoporous molecular sieves, the calcination technique was used. In this procedure, each sample was subjected to heating from room temperature to 500°C under a dynamic nitrogen atmosphere with a flow of 100 mL min^{-1} and a heating rate of 10°C min^{-1}. Upon reaching 500°C, each material remained for one hour under nitrogen in the same flow. After this time, the gas was changed to synthetic air (reactive gas), and heated at the sample temperature for another hour, with a flow of 100 mL min^{-1}. The supports were called SBA-15 and AlSBA-15.

3.2. Preparation of the CoMo/SBA-15 and CoMo/AlSBA-15.

Co and Mo metals were deposited on mesoporous supports using the impregnation technique with excess solvent using absolute ethanol: C_2H_5OH (99.5%, Merck) as solvent; cobalt nitrate hexahydrate: $Co(NO_3)_2.6H_2O$ (99%, Merck) as a source of cobalt and ammonium heptamolybdate tetrahydrate: $(NH_4)_6Mo_7O_{24}.4H_2O$ (Ecibra, 82.5% in MoO_3) as a source of molybdenium. Before impregnation, all mesoporous supports were subjected to a TG run in a nitrogen atmosphere at a heating rate of 20°C min^{-1} from 30 to 900 °C, with the aim of determining the relative humidity levels of each support, the starting from mass losses in the range of 30 to 130°C, and using this data to correct the dry mass of the supports in order to minimize weighing errors during the deposition stage of the cobalt and molybdenum precursor salts.

The metal impregnation procedure consisted of weighing the mass of the support considering the relative humidity. The necessary amounts of cobalt nitrate and ammonium hepatmolybidate were weighed in a porcelain crucible and solubilized in 2 mL of absolute ethanol using a glass rod. After solubilization of the salts, the support was slowly added, stirring with the glass rod. The crucible with the suspension was transferred to the heating mantle at 70 °C, homogenizing periodically to evaporate the excess solvent. After evaporation of excess ethanol, the crucible was transferred to the oven and dried at 100 °C for 6 hours. The depositions of the metallic phases were carried out to obtain a loading of 15% by weight of active phase, with a [Co/(Co+Mo)] atomic ratio of 0.45.

3.3. Physicochemical characterization of the obtained materials.

3.3.1. Thermogravimetry (TG)

 doi:10.20944/preprints202401.1954.v1

Thermal analysis using TG was used to carry out studies to determine the best calcination conditions for eliminating P123 from the pores of mesoporous materials SBA-15 and AlSBA-15, as well as verifying the best calcination conditions for decomposition of the precursor salts of the metallic phases of cobalt and molybdenum. Thermogravimetric analyzes of the as-synthesized mesoporous materials (SBA-15 and AlSBA-15) were obtained in a thermobalance with a horizontal furnace model TA/SDTA 951 from Mettler. The thermogravimetric curves of the non-calcined samples were obtained by heating the sample from room temperature to 900 ^{o}C in a dynamic nitrogen atmosphere at three heating rates of 5, 10 and 20 ^{o}C min^{-1}, with the aim of carrying out a series of kinetic studies regarding the best conditions for removing the P123 template from the pores of the materials and thus establishing the best calcination conditions. For each test, alumina crucibles with a mass of around 10 mg were used.

By using TG, it was possible to study the best conditions for calcining mesoporous materials impregnated with cobalt and molybdenum salts. In all cases, approximately 10 mg of each non-calcined sample was heated from room temperature to 900^{o}C at a heating rate of 10 ^{o}C min^{-1}. The curves were obtained in a dynamic synthetic air atmosphere of 25 mL min^{-1}.

3.3.2. X-ray diffraction (XRD)

XRD analyzes using the powder method were carried out on materials obtained in calcined form, with the aim of verifying whether the mesoporous hexagonal structure had formed. In the samples impregnated after the calcination process, new XRD analyzes were carried out to verify variations in the hexagonal mesoporous structure and to identify the crystalline phases of the cobalt and molybdenum oxides formed.

The X-ray diffractograms of the SBA-15 and AlSBA-15 samples were obtained in an angular scan of 0.5 to 5.0 degree on a Shimadzu model XRD 6000 equipment. The tests were conducted using CuKα radiation and a nickel filter with a tube voltage of 30 kV and current of 30 mA. The slit had an opening of 0.15 degree and the X-ray beam was phased in relation to the sample with a speed of 0.5 degree/min and a step of 0.01 degree. For samples containing deposited cobalt and molybdenum oxides, XRD were carried out in an angular range of 5 to 60 degree.

3.3.3. Nitrogen adsorption

The specific surface area, determined by the BET method, total pore volume, distribution and average pore size diameter, were determined through N_2 adsorption at the temperature of liquid N_2 (77 K). The experiments of the adsorption isotherms of the calcined samples were carried out on a Micromeritics ASAP2010 equipment. To this end, approximately 100 mg of each sample was previously treated at 170 ^{o}C for 12 hours under vacuum and then subjected to nitrogen adsorption at 77 K. The adsorption and desorption isotherms were obtained in a relative pressure (P/P_o) range of 0.01 to 0.95. The data relating to the volume of adsorbed gas as a function of partial pressure were correlated using mathematical models to determine the BET surface area [57], and BJH to volume and distribution of pores [58].

3.3.4. Scanning electron microscopy (SEM)

Scanning electron micrographs of the mesoporous supports SBA-15 and AlSBA-15 with Si/Al=50, as well as the supported cobalt and molybdenium catalysts were carried out with the aim of observing the morphology of the synthesized mesoporous materials and some change in the morphology after impregnation the CoMo metals. The analysis were obtained using a Jeol equipment model JSM-5610 LV. Before analysis, the samples were adhered to the sample holder using a thin carbon tape and subjected to a pre-treatment that consisted of the deposition of a thin nanolayer of gold, with the aim of making the sample a good electron conductor and thus be able to provide good quality and resolution of the images. The analyzes were carried out with magnifications ranging from 100 to 25,000 times.

3.4. Thiophene Hydrodesulfurization (HDS)

 doi:10.20944/preprints202401.1954.v1

The thiophene HDS catalytic tests were carried out in a fixed bed continuous flow reactor, under atmospheric pressure, according to the scheme shown in Figure 16. Thiophene was chosen as a probe molecule, which is characterized as the most common sulfur contaminant present in middle petroleum distillates. To carry out the tests, approximately 50 mg of sample was introduced into the Pyrex glass "U" reactor heated from room temperature to 450°C at a heating rate of 5 °C min^{-1} in a dynamic atmosphere of N_2 containing 10% of H_2 with a total flow of 30 mL min^{-1}. After reaching 450 °C, the sample remained under these conditions for another 1 hour and was then cooled to the reaction temperature of 350 °C, still maintaining the reducing atmosphere. Then a mixture of n-heptane containing 12070 ppm of thiophene (ca. 5100 ppm of sulfur) was drawn from a saturator maintained at room temperature through a line heated at 120 °C to the catalytic bed with a flow of 30 mL min^{-1}, maintaining the molar ratio H_2/(thiophene and n-heptane) of 8.2. The composition of the standard mixture of thiophene in n-heptane was confirmed through chemical analysis using an EDX-700 equipment (Shimadzu).

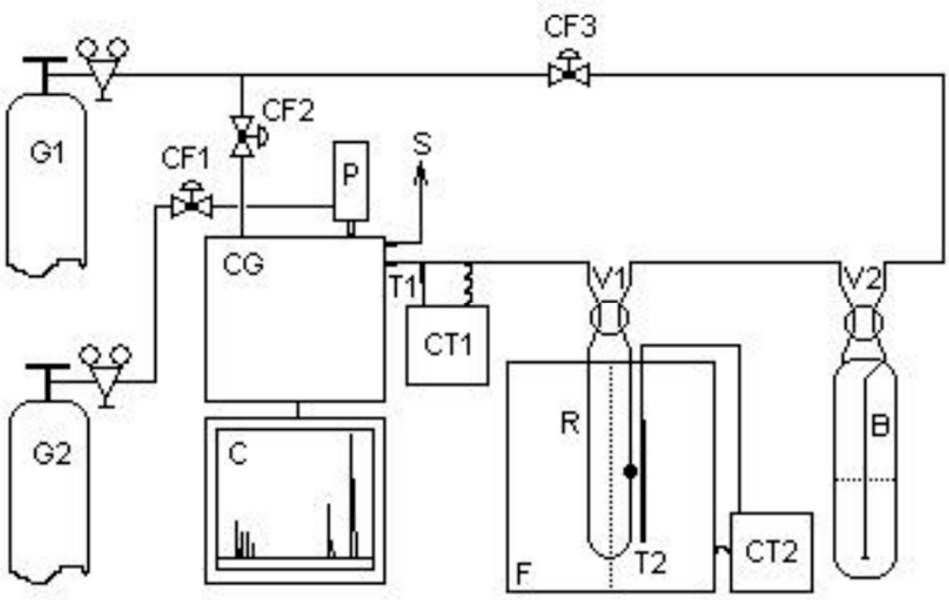

Figure 16. Catalytic evaluation unit. Where: G1 = hydrogen; G2 = nitrogen; V1, V2, = 4-way valves; CF1, CF2, CF3 = flow control valves; B = saturator; P = 10-way pneumatic valve; CT1, CT2 = temperature controllers; T1, T2 = thermocouples; S = gas output; C = chromatogram; GC = gas chromatograph; F= furnace and R = reactor with catalyst.

During the reaction, the catalytic bed was maintained at a constant temperature of 350 °C using a COEL HW1500 temperature controller. The reactor effluent products were successively injected "on-line" through a ten-way valve into a Varian CP3800 gas chromatograph with thermal conductivity detector at 15-minute intervals until reaching the pseudo-stationary state. The products were separated and analyzed in a 60m fused silica column. The identification of products was carried out by comparing the retention times of the analytes of each chromatogram with the retention times of thiophene, n-heptane and natural gas standards, considering the elution orders of the substances through the stationary phase used in the column (separation based on boiling points) as proposed by the manufacturer. Quantification of chromatogram peaks was performed using the method of external standards analyzed in the linearity range of the detector as recommended for thermal conductivity detectors. The tests were conducted with all catalysts in powder form, to minimize the effects arising from internal mass transport. The following aspects were also taken into consideration: isothermal reaction in a fixed bed, vapor phase in an ideal gas state, uniform porosity and negligible pressure drop in the bed without the presence of axial dispersion effects.

4. Conclusions

The effect of mesoporous supports such as silica (SBA-15), and aluminosilicate (AlSBA-15) on catalytic activities of cobalt and molybdenum (CoMo) catalysts was demonstrated for thiophene hydrodesulfurization in n-heptane stream as model reaction. The characterization of the mesoporous supports by nitrogen adsorption-desorption analysis showed that SBA-15 and AlSBA-15 (Si/Al=50) materials possessed surface area, pore diameter and pore volume appropriate for impregnation and dispersion of the Co and Mo metals on the surface. The crystallization properties by X-ray diffraction analysis showed that the Co and Mo metals were well dispersed in the catalytic supports. The catalytic activities indicated that the ordering and open pore channel of the CoMo/SBA-15 and CoMo/AlSBA-15 mesoporous catalysts are appropriate for thiophene conversion and selectivity to paraffin butane, and olefins 1-butene, cis- and trans- 2-butene. The 1,3-butene and tetrahydrothiophene (THT) molecules were not de-detected in the products, evidencing that these compounds are strongly adsorbed on the Co-Mo active sites and undergo hydrogenation and desulfurization, respectively, with subsequent formation of C_4-paraffins, such as n-butane and isobutane.

The catalytic activity of CoMo/SBA-15 for thiophene HDS reaction was higher than that of CoMo/AlSBA-15, reaching ca. 20 and 30% conversion, respectively, after 1 hour of reaction. The same trend was observed for the paraffin/olefin ratio. Therefore, using the CoMo/SBA-15 catalyst, after 1 hour of reaction, the paraffin/olefin ratio increased from 0.2 to 0.3 up to 2 hours of reaction. With the CoMo/AlSBA-15 catalyst, it was found that this ratio remained constant between 1 and 2 hours of reaction, with a value lower than 0.1, showing that the AlSBA-15 support stabilized the structure. Regarding product selectivity, in general the two catalysts were selective for the olefins 1-butene, trans- and cis-2-butenes. In relation to paraffins, for the CoMo/SBA-15 catalyst, ca. 10% selectivity was obtained for isobutane and n-butane. On the other hand, using the CoMo/AlSBA-15 catalyst, low concentrations of paraffins were observed, with a subsequent increase in the concentration of 1-butene, showing that the n-butane dehydrogenation reaction caused by metallic sites probably occurred, and isomerization to iso-butane, due to the presence of Bronsted acid sites generated by Al in the CoMo/AlSBA-15 catalyst.

Author Contributions: Conceptualization, A.C.S.L.S.C.; and J.M.F.B.; methodology, A.C.S.L.S.C. and M.J.B.S.; formal analysis, M.D.S.A. and J.B.S.; investigation and data curation, A.C.S.L.S.C.; data curation, writing—original draft preparation, A.S.A.; writing—review and editing, M.D.S.A., A.S.A. and J.B.S.; project administration, A.S.A. and V.J.F.; funding acquisition, ASA. All authors have read and agreed to the published version of the manuscript.

Funding: This research was funded by CNPq, grant number 312461/2022-4.

Data Availability Statement: Not applicable.

Acknowledgments: The authors thank the Brazilian Agency of Petroleum, Natural Gas and Biofuel (ANP), and National Council for Scientific and Technological Development (CNPq Brazil, Grant number 312461/2022-4), for support this research.

Conflicts of Interest: The authors declare no conflict of interest.

References

1. Ohtsuka, T., Catalyst for hydrodesulfurization of petroleum residua, *Catal. Rev. Sci.- Eng*., **1997**, *16*, 291–325.
2. Delmon, B.; Li, Y. W., Modeling of hydrotreating catalysts based on the remote control: HYD e HDS, *J. Mol. Catal. A: Chem*., **1997**, *127*, 163–190.
3. Topsoe, H.; Clausen, B. S., Importance of Co-Mo type structures in hydrodesulfurization. *Catal. Rev. Sci.-Eng*., **1984**, *26*, 395–420.
4. Topsoe, H., Characterization of the structures and active sites in sulfided Co-Mo/Al_2O_3 and Ni-Mo/Al_2O_3 catalysts by NO chemiosorption, *J. Catal*., **1983**, *84*, 386–401.

5. Grande. P.; Vanhaeren, X. Hydrotreating catalysts, an old story with new challenges, *Catal. Today*, **1997**, *36*, 375–391.
6. Morais, C.G.D.P.; Silva, J.B.; Almeida, J.S.; Oliveira, R.R.; Araujo, M.D.S.; Fernandes, G.J.T.; Delgado, R.C.O.B.; Coriolano, A.C.F.; Fernandes, V.J., Jr.; Araujo, A.S. Catalytic Distillation of Atmospheric Residue of Petroleum over HY-MCM-41 Micro-Mesoporous Materials. *Catalysts* **2023**, *13*, 296.
7. Yue, L., Li, G.; Zhang, F.; Chen, L.; Li, X.; Huang, X. Size-dependent activity of unsupported Co–Mo sulfide catalysts for the hydrodesulfurization of dibenzothiophene, *Appl. Catal. A: Gen.* **2016**, *512*, 85–92.
8. Zepeda, T.A.; de Leon, J.N.D.; Alonso, G.; Infantes-Molina, A.; Galindo-Ortega, Y.I.; Huirache-Acuna, R.; Fuentes, S. Hydrodesulfurization activity of Ni-containing unsupported Ga(x)WS_2 catalysts, *Catal. Commun*. **2019**, *130*, 105760.
9. Morales-Ortuno, J.C.; Ortega-Domínguez, R.A.; Hernandez-Hipolito, P.; Bokhimi, X.; Klimova, T.E. HDS performance of NiMo catalysts supported on nanostructured materials containing titania, *Catal. Today*, **2016**, *271*, 127–139.
10. Shang, H.; Liu, C.; Xu, Y.; Qiu, J.; Wei, F. States of carbon nanotube supported Mo based HDS catalysts, *Fuel Process. Technol*. **2007**, *88*, 117–123.
11. Liu, Z.; Zhang, L.; Jiang, J.; Bian, C.; Zhang, Z.; Gao, Z. Advancement of hydrodesulfurization catalyst and discussion of its application in coal tar, *Adv. Chem. Eng*. **2013**, *03*, 36–46.
12. Umar, M.; Abdulazeez, I.; Tanimu, A.; Ganiyu, S.A.; Alhooshani, K. Modification of ZSM-5 mesoporosity and application a catalyst support in hydrodesulfurization of dibenzothiophene: experimental and DFT studies, *J. Environ. Chem. Eng*. **2021**, *9* 106738.
13. Yu, Q.; Zhang, L.; Guo, R.; Sun, J.; Fu, W.; Tang, T.; Tang. T. Catalytic performance of CoMo catalysts supported on meso rous ZSM-5 zeolite-alumina composites in the hydrodesulfurization of 4,6-dimethyldibenzothiophene, *Fuel Process. Technol*. **2017**, *159*, 76–87.
14. Qi, L.; Zheng, P.; Zhao, Z.; Duan, A.; Xu, C.; Wang, X. Insights into the intrinsic kinetics for efficient hydrodesulfurization of 4,6-dimethyldibenzothiophene over mesoporous $CoMoS_2$/ZSM-5, *J. Catal.*, **2022**, *408*, 279–293.
15. Zhou, W.; Zhou, A.; Zhang, Y.; Zhang, C.; Chen, Z.; Liu, L.; Zhou, Y.; Wei, Q.; Tao, X. Hydrodesulfurization of 4,6-dimethyldibenzothiophene over NiMo supported on Ga-modified Y zeolites catalysts, *J. Catal.*, **2019**, *374*, 345–359.
16. Song, H.; Wang, J.; Wang, Z.; Song, H.; Li, F.; Jin, Z. Effect of titanium content on dibenzothiophene HDS performance over Ni_2P/Ti-MCM-41 catalyst, *J. Catal.*, **2014**, 311, 257–265.
17. Souza, M.J.B.; Marinkovic, B. A.; Jardim, P. M.; Araujo, A. S.; Pedrosa, A.M.G.; Souza, R.R. HDS of thiophene over CoMo/AlMCM-41 with different Si/Al ratios. *Appl. Catal. A: Gen.* **2007**, *316*, 212–218.
18. Calderon-Magdaleno, M.A.; Mendoza-Nieto, J.A.; Klimova, T.E. Effect of the amount of citric acid used in the preparation of NiMo/SBA-15 catalysts on their performance in HDS of dibenzothiophene-type compounds, *Catal. Today*, **2014**, 220-222, 78–88.
19. Soni, K.K.; Chandra Mouli, K.; Dalai, A.K.; Adjaye, J. Effect of Ti loading on the HDS and HDN activity of KLGO on NiMo/TiSBA-15 catalysts, *Microp. Mesop. Mater*. **2012**, *152*, 224–234.
20. Alonso-Perez, M.O.; Pawelec, B.; Zepeda, T.A.; Alonso-Núnez, G.; Nava, R.; Navarro, R. M.; Huirache-Acuna, R. Effect of the titanium incorporation method on the morphology and HDS activity of supported ternary Ni–Mo–W/SBA-16 catalysts, *Microp. Mesop. Mater*. **2021**, *312*, 110779.
21. Dominguez Garcia, E.; Chen, J.; Oliviero, E.; Oliviero, L.; Mauge, F. New insight into the support effect on HDS catalysts: evidence for the role of Mo-support interaction on the MoS_2 slab morphology, *Appl. Catal. B: Environ*., **2020**, *260*, 117975.
22. Roy, T.; Rousseau, J.; Daudin, A.; Pirngruber, G.; Lebeau, B.; Blin, J.-L.; Brunet, S. Deep hydrodesulfurization of 4,6-dimethydibenzothiophene over CoMoS/TiO2 catalysts: Impact of the TiO2 treatment, *Catal. Today*, **2021**, *377*, 17–25.
23. Mazurelle, J.; Lamonier, C.; Lancelot, C.; Payen, E.; Pichon, C.; Guillaume, D. Use of the cobalt salt of the heteropolyanion $[Co_2Mo_{10}O_{38}H_4]_6$ for the preparation of CoMo HDS catalysts supported on Al_2O_3, TiO_2 and ZrO_2, *Catal. Today*, **2008**, *130*, 41–49.
24. Zhang, L.; Chen, Z.; Zheng, S.; Cai, G.; Fu, W.; Tang, T.; He, M. Effect of the Co/Mo Ratio on the Morphology and Activity of the CoMo Catalyst Supported on MgO Nanosheets in Dibenzothiophene Hydrodesulfurization, *Ind. Eng. Chem. Res*., **2020**, *59*, 12338–12351.

25. Bing, L.C.; Tian, A.X.; Li, J.J.; Yi, K.F.; Wang, F.; Wu, C.Z.; Wang, G.J. The effects of chelating agents on CoMo/TiO_2-Al_2O_3 hydrodesulfurization catalysts, *Catal. Lett*. **2018**, *148*, 1309–1314.
26. Li, G.; Li, W.; Zhang, M.; Tao, K. Characterization and catalytic application of homogeneous nano-composite oxides ZrO_2–Al_2O_3, *Catal. Today*, **2004**, 93-95, 595–601.
27. Tavizon Pozos, J.A.; Esquivel, G.C.; Cervantes Arista, I.; de los Reyes Heredia, J.A.; Suarez Toriello, V.A. Co-processing of hydrodeoxygenation and hydrodesulfurization of phenol and dibenzothiophene with NiMo/Al_2O_3–ZrO_2 and NiMo/TiO_2–ZrO_2 catalysts, *Int. J. Chem. React. Eng*. **2022**, *20*, 47–60.
28. Kazakov, M.O.; Kazakova, M.A.; Vatutina, Y.V.; Larina, T.V.; Chesalov, Y.A.; Gerasimov, E. Y.; Prosvirin, I.P.; Klimov, O.V.; Noskov, A.S. Comparative study of MWCNT and alumina supported CoMo hydrotreating catalysts prepared with citric acid as chelating agent, *Catal. Today*, **2020**, 357, 221–230.
29. Saleh, T.A. Carbon nanotube-incorporated alumina as a support for MoNi catalysts for the efficient hydrodesulfurization of thiophenes, *Chem. Eng. J*. **2021**, *404*, 126987.
30. Saleh, T.A.; Al-Hammadi, S.A.; Abdullahi, I.M.; Mustageem, M. Synthesis of molybdenum cobalt nanocatalysts supported on carbon for hydrodesulfurization of liquid fuels, *J. Mol. Liq*. **2018**, *272*, 715–721.
31. Prajapati, Y.N.; Verma, N. Hydrodesulfurization of thiophene on activated carbon fiber supported NiMo catalysts, *Energy Fuel*, **2018**, *32*, 2183–2196.
32. Abubakar, U.C.; Alhooshani, K.R.; Adamu, S.; Al Thagfi, J.; Saleh, T.A. The effect of calcination temperature on the activity of hydrodesulfurization catalysts supported on mesoporous activated carbon, *J. Clean. Prod*. **2019**, *211*, 1567–1575.
33. Ali, I.; Al-Arfaj, A.A.; Saleh, T.A. Carbon nanofiber-doped zeolite as support formolybdenum based catalysts for enhanced hydrodesulfurization of dibenzothiophene, *J. Mol. Liq*. **2020**, *304*, 112376.
34. Araujo, A.S.; Quintella, S.A.; Coutinho, A.C.S.L.S. Synthesis monitoring of SBA-15 nanostructured materials. *Adsorption*, **2009,** *15*, 306–311.
35. Antochshuk, V.; Araujo, A.S.; Jaroniec, M. Functionalized MCM-41 and CeMCM-41 materials synthesized via interfacial reactions. *J. Phys. Chem. B*, **2000**, *104*, 9713–9719.
36. Araujo, A.M.M.; Queiroz, G. S.; Maia, D.O.; Gondim, A. D.; Souza, L.D.; Fernandes Jr., V.J.; Araujo. Fast Pyrolysis of Sunflower Oil in the Presence of Microporous and Mesoporous Materials for Production of Bio-Oil. *Catalysts*, **2018**, *8*, 261.
37. Araujo A.S.; Jaroniec M. Determination of the surface area and mesopore volume for lanthanide-incorporated MCM-41 materials by using high resolution thermogravimetry. *Thermochim. Acta*, **2000**, *345*, 173–177.
38. Barros, J.M.F.; Fernandes, G.J.T.; Araujo, M.D.S.; Melo, D.M.A.; Gondim, A.D.; Fernandes, V.J., Jr.; Araujo, A.S. Hydrothermal Synthesis and Properties of Nanostructured Silica Containing Lanthanide Type Ln–SiO2 (Ln = La, Ce, Pr, Nd, Eu, Gd, Dy, Yb, Lu). *Nanomaterials* **2023**, *13*, 382.
39. Araujo, A.S., Jaroniec, M. Synthesis and properties of lanthanide incorporated mesoporous molecular sieves (1999) *J. Colloid. Interf. Sci.*, **1999**, *218*, 462–467.
40. Coutinho, A.C.S.L.S; Quintella, S.A.; Araujo A.S.; Barros, J.M.F.; Pedrosa, A.M.G.; Fernandes Jr., V.J.; Souza M.J.B. Thermogravimetry applied to characterization of SBA-15 nanostructured material. *J. Therm. Anal. Calorim.* **2007**, *87*, 457–461.
41. Souza M.J.B.; Silva A.O.S.; Aquino, J.M.F.B.; Fernandes Jr. V.J.; Araujo A.S. Kinetic study of template removal of MCM-41 nanostructured material. *J. Therm. Anal. Calorim*. **2004**, *75*, 693–698.
42. Araujo, A. S.; Fernandes Jr., V. J.; Souza, M. J.B.; Silva, A. O.S.; Aquino, J. M.F.B. Model free-kinetics applied to CTMA+ removal of AlMCM-41 molecular sieves. *Thermochim. Acta*, **2004**, *413*, 235–2408.
43. Araujo S.A.; Ionashiro M.; Fernandes Jr., V.J.; Araujo A.S. Thermogravimetric investigations during the synthesis of silica-based MCM-41. *J. Therm. Anal. Calorim.* **2001**, *64*, 801–805.
44. Souza, M.J.B.; Lima, Stevie H.; Araujo, A.S.; Pedrosa, A.M.G.; Coutinho, A.C.S.L.S. Determination of the acidity of MCM-41 with different Si/A1 ratios by the temperature programmed desorption of pyridine. *Ads. Sci. Techn.*, **2007**, *25*, 751–756.
45. Araujo, A. S.; Souza, C.D.R.; Souza, M. J. B.; Fernandes Jr, V. J.; Pontes, L.A.M. Acid properties of ammonium exchanged A1MCM-41 with different Si/Al ratio. *Stud. Surf. Sci. Catal.* **2002**, *141*, 467–472.
46. Farias, M. F.; Domingos, Y. S.; Fernandes, G.J.T.; Castro, F. L.; Fernandes Jr., V.J.; Costa, M.J.F.; Araujo, A.S. Effect of acidity in the removal-degradation of benzene in water catalyzed by Co-MCM-41 in medium containing hydrogen peroxide. *Microp. Mesop. Mater.* **2018**, *258*, 33–40.

47. Coriolano, A. C. F.; Barbosa, G. F. S.; Alberto, C. K. D.; Delgado, R. C. O. B.; Castro, K. K. V.; Araujo, A. S. Catalytic processing of atmospheric residue of petroleum over AlSBA-15 nanomaterials with different acidity. *Petrol. Sci. Techn.*, **2016**, *34*, 627–632.
48. Gajardo, J., Colmenares-Zerpa, J., Peixoto, A.F., Silva, D.S.A., Silva, J.A., Gispert-Guirado, F., Llorca, J., Chimentão, R.J. Revealing the effects of high Al loading incorporation in the SBA-15 silica mesoporous material. 2023, *J. Porous Mat.* **2023**, *5*, 1687–1707.
49. Fernandes Jr., V.J.; Araujo A.S.; Fernandes G.J.T. Thermal analysis applied to solid catalysts. Acidity, activity and regeneration. *J. Therm. Anal. Calorim.* **1999**, *56*, 275–285.
50. Zhao, D.; Hou, Q.; Feng, J.; Chmelka, B. F.; Stucky, G. D., Nonionic triblock and star diblock copolymer and oligomeric surfactant syntheses of highly ordered, hydrothermally stable, mesoporous silica structures. *J. Am. Chem. Soc.*, **1998**, *120*, 6024–6036.
51. Zhao, D.; Feng, J.; Hou, Q.; Melosh, N.; Fredrickson, G. H.; Chmelka, B. F.; Stucky, G. D., Triblock copolymer syntheses of mesoporous silica with periodic 50 to 300 angstrom pores, *Science*, **1998**, *279*, 548–552.
52. Han, Y. J.; Kim, J. M.; Stucky, G. D., Preparation of nobel metal nanowires using hexagonal mesoporous silica SBA-15, *Chem. Mater.*, **2000**, *12*, 2068–2069.
53. Dhar, G. M.; Kumaran, G. M.; Kumar, M.; Rawat, K.S.; Sharma, L. D.; Raju, B. D.; Rao, K. S. R., Physico-chemical characterization and catalysis on SBA-15 supported molybdenum hydrotreating catalysts, *Catal. Today*, **2005**, *99*, 309–314.
54. Kumaran, G. M.; Garg, S.; Soni, K.; Kumar, M.; Sharma, L. D.; Dhar, G. M.; Rao, K. S. R., Effect of Al-SBA-15 support on catalytic functionalities of hydrotreating catalysts I. Effect of variation of Si/Al ratio on catalytic functionalities, *Appl. Catal. A: Gen.*, **2006**, *305*, 123–129.
55. Tuel, A.; Hubert-Pfalzgraf, L. G., Nanometric monodispersed titanium oxide particles on mesoporous silica: synthesis, characterization and catalytic activity in oxidation reactions in the liquid phase, *J. Catalysis*, **2003**, *217*, 343–353.
56. Thommes, M.; Kaneko, K.; Neimark, A.V.; Olivier, J.P.; Rodriguez-Reinoso, F.; Rouquerol, J.; Sing, K.S.W. Physisorption of Gases, with Special Reference to the Evaluation of Surface Area and Pore Size Distribution (IUPAC Technical Report). *Pure Appl. Chem.* **2015**, *87*, 1051–1069.
57. Brunauer, S.; Emmett, P. H.; Teller, E., Adsorption of gases in multimolecular layers, *J. Am. Chem. Soc.*, **1938**, *60*, 309–319.
58. Barrett, E.P.; Joyner, L.G.; Halenda, P.P. The determination of pore volume and area distributions in porous substances. I. Computations from nitrogen isotherms. *J. Am. Chem. Soc.* **1951**, *73*, 373–380.
59. Eswaramoorthi, I.; Dalai, A. K., Synthesis, characterization and catalytic performance of boron substituted SBA-15 molecular sieves, *Microp. Mesop. Mat.*, **2006**, *93*, 1–11.
60. Vinu, A.; Kumar, G. S.; Ariga, K.; Murugesan, V., Preparation of highly ordered mesoporous AlSBA-15 and its application to isopropylation of m-cresol, *J. Mol. Catal. A*, **2005**, *235*, 57–66.
61. Gédéon, A.; Lassoued A.; Bonardet, J. L.; Fraissard, J., Surface acidity diagnosis and catalytic of AlSBA materials obtained by direct synthesis, *Microp. Mesop. Mat.*, **2001**, *801*, 44–45.
62. Ooi, Y. S.; Zakaria, R.; Mohamed, A. R.; Bhatia, S., Hydrothermal stability and catalytic activity of mesoporous aluminum-containing SBA-15, *Catalysis Comm.*, **2004**, *5*, 441–445.
63. Chao, M. C.; Lin, H. P.; Sheu, H. S.; Mou, C. Y., A study of morphology of mesoporous silica SBA-15. *Stud. Surf. Sci. Catal.* **2002**, 141, 387–394.
64. Choi, D. G.; Yang, S. M., Effect of two-step sol-gel reaction on the mesoporous silica structure, *J. Col. Interf. Sci.*, **2003**, *261*, 127–132.
65. Katiyar, A.; Yadav, S.; Smirniotis, P.; Pinto, N. G., Synthesis of ordered large pore SBA-15 spherical particles for adsorption of biomolecules, *J. Chromatography A*, **2006**, *1-2*, 13–20.
66. Wang, E.; Yang, F.; Song, M.; Chen, G.; Zhang, Q.; Wang, F.; Bing, L.; Wang, G.; Han, D. Recent advances in the unsupported catalysts for the hydrodesulfurization of fuel. *Fuel Proc. Techn.* **2022**, 235, 107386.
67. Lauritsen J.V.; Besenbacher, F. Atom-resolved scanning tunneling microscopy investigations of molecular adsorption on MoS2 and CoMoS hydrodesulfurization catalysts. *J. Catalysis*, **2015**, *328*, 49–58.
68. Tétényi, P.; Szarvas, T.; Ollár, T. Experimental proof of thiophene hydrodesulfurization reaction steps by isotope (14C) labeled thiophene. *React. Kinet. Mechan. Catal.* **2021**, *134*, 697–710
69. Desikan, P.; Amberg, C. H., Catalytic hydrodesulphurization of thiophene. Selective poisoning plus acidity of catalyst surface, *Can. J. Chem.*, **1964**, *42*, 843–850.

70. Iwamoto, R.; Inamura, K.; Nozaki, T.; Lino, A., Effect of cobalt on the sulfiding temperature of CoO-MoO_3/Al_2O_3 studied by temperature programmed sulfiding. *Appl. Catal. A: Gen*., **1997**, *163*, 217–225.
71. Delmon, B.; Li, Y. W., Modeling of hydrotreating catalysts based on the remote control: HYD e HDS, *J. Mol. Catal. A: Chem*., **1997,** *127*, 163–190.
72. Yamada, T.; Zhou, H.; Asai, K.; Honma, I., Pore size controlled mesoporous silicate powder prepared by triblock copolymer templates, *Mater. Letters*, **2002**, *56*, 93–96.